FACHHOCHSCHULE **TRIER**
Hochschule für Technik, Wirtschaft und Gestaltung
University of Applied Sciences
Informatik

Informatik-Bericht Nr. 2010-5

Schriftenreihe Fachbereich Informatik, Fachhochschule Trier

MER FEATURE ANALYSIS AND SELECTION FOR COMPUTER-AIDED GPE/GPI NAVIGATION

Yannick Thesen and Peter Gemmar
Institute for Innovative Informatics Applications i3A
University of Applied Sciences (FH) Trier
Schneidershof, 54293 Trier, Germany
email: y.thesen@fh-trier.de

Dr. Frank Hertel
Service de Neurochirurgie
Centre Hospitalier de Luxembourg
4, Rue Barblé, L-1210 Luxembourg
email: hertel.frank@chl.lu

ABSTRACT
Using microelectrode recordings (MER) to aid the navigation of stimulation electrodes to the optimal target position during deep brain stimulation (DBS) surgery in patients suffering from Parkinson's disease proved effective in the past and has become common practice. In recent years, pallidal DBS for severe cases of dystonia with the internal part of the globus pallidus (GPi) as the preferred stimulation target has become increasingly popular. However, recordings from dystonic patients have been found to be less conclusive in delineating the target structure from its surroundings.

We studied microelectrode recordings obtained from 19 patients undergoing surgery for pallidal DBS and observed several types of recordings exhibiting distinct firing characteristics. Various features were extracted and analyzed in order to find measures that characterize these signal types. Using statistic analysis and Self-Organizing Maps (SOMs), those features allowing the best separation between non-neuronal and neuronal recordings were identified. The information gained was used to generate a fuzzy classifier which is capable of differentiating between MERs of the two classes in most of the cases.

KEY WORDS
Biomedical Signal Processing, Dystonia, Deep Brain Stimulation, Self-Organizing Maps, Feature Extraction, GPi.

1 Introduction

Deep brain stimulation (DBS) is a common treatment option for people suffering from Parkinson's disease, essential tremor, dystonia and other neurological disorders, especially in cases where medical treatment is unsuccessful. DBS is a sophisticated procedure requiring thorough planning and a high level of accuracy when implanting the electrodes, in order to minimize the risk of damaging critical structures and blood vessels and to improve chances of a successful treatment. An essential task in the stereotactic implant procedure is the navigation of the microelectrodes to the calculated target coordinates as well as the determination of the optimal stimulation site and the subsequent verification of the electrode positions.

A widely-used technique to improve targetting with good reported clinical outcome [1, 2, 3, 4, 5] is the intraoperative analysis of microelectrode recordings (MER). Neuronal activity is recorded at each depth along the trajectory while advancing the electrode into the brain. The surgeon can then, based on his knowledge of characteristic signal properties from different functional areas, confirm or correct the current position of the electrode tip.

To aid the surgeon in placing the electrodes, there exists an effort to find signal features and analysis methods that allow a more objective mapping of microelectrode recordings to functional areas, which could then be used in an automatic navigation assistant. Apart from improving clinical outcomes of DBS, such a tool could help make the procedure safer and less time consuming, thereby reducing the strain of the operation on patient and surgeon alike.

In the case of Parkinson's disease, the preferred target for DBS is the subthalamic nucleus (STN) located in the basal ganglia. A typical electrode trajectory passes through the thalamus and the zona incerta (ZI) into the STN before entering the substantia nigra (SNr). The signals recorded from different regions on the electrode's path show distinct properties that are well documented [2, 6, 7] and that allow for a rather straight-forward detection of STN borders.

At our institution, we already developed an automatic classifier for recordings from thalamic DBS in Parkinson patients, which is capable of distinguishing between the STN and the surrounding brain structures, the classifications being consistent with manual decisions by an experienced surgeon in more than 96% of cases [8].

In recent years, DBS has become a more common treatment option for patients suffering from dystonia, a neurological movement disorder in which sustained muscle contractions cause twisting and repetitive movements or abnormal postures. While medical treatment (mostly with local injections of Botolinum toxin) is possible and this form of therapy offers some relief, generalized dystonias are difficult to treat with medication and resistances or side effects are common.

The primary stimulation target for DBS in dystonia patients is the globus pallidus pars interna (GPi), which is part of the globus pallidus, a fairly large sub-cortical structure located in the basal ganglia that is divided by the medial medullary lamina into an external and an internal part (GPe and GPi). Unlike with thalamic or pallidal DBS in

Parkinson's disease, microelectrode recordings from pallidal DBS for dystonia have proven less conclusive in delineating the target structure from its surroundings because of the apparent similarities of firing patterns in GPi and GPe and the spontaneous nature of discharges in both nuclei [1, 9, 10, 11, 12, 13]. Electrode placement in dystonic patients is complicated further by the fact that (1) the GPi is a relatively large structure and the optimal target location is difficult to determine, (2) stimulation effects are not immediately visible as is the case with Tremor where intraoperative test stimulation is applied to verify the electrode position and (3) dystonia surgery is typically performed under general anesthesia, which may influence the appearance of microelectrode recordings [14].

Here we present our findings regarding characteristics of microelectrode recordings obtained from 19 dystonia patients undergoing stereotactic surgery for pallidal deep brain stimulation. As a first step to developing a navigation assistant, we investigated means of automatically identifying MERs of different appearances. Several signal features were considered to find those most suitable for classifying recordings into neuronal and non-neuronal. Self-Organizing Maps were used to detect features that are relevant as well as those that are irrelevant or redundant for this task. As a first result, a fuzzy classifier which shows promising performance is presented and further research steps are discussed.

2 Material and Methods

2.1 Equipment, Recording Techniques and Patients

The recordings used in our research were obtained during surgery for pallidal DBS in 19 patients suffering from various forms of dystonia treated at the hospital of Idar-Oberstein, Germany, using microelectrodes, microdrive and Leadpoint^{TM}from Medtronic Inc, Minneapolis, Minnesota, USA. All of the MERs had a length of 10 seconds with a sample rate of 24 kHz. MERs were recorded every millimeter along the electrode's trajectory (every 0.5 mm in target proximity). All surgeries were performed under general anesthesia.

2.2 Characteristics of Microelectrode Recordings

As expected, the recordings encountered along the electrode trajectories displayed a broad variety in appearance and showed no obvious patterns among different patients. Because of this variability, it was seldom possible to visually group adjacent recordings in a way that would allow implications regarding the underlying neuronal structures. Based on observations made by others (e.g. [1, 2, 11]) and on our own investigations, we identified several recording types that may help in further characterizing these MERs (figure 1):

- *Non-neuronal*: Signals show no or little spikes and mostly low background noise. Artifacts or single detached spikes may occur.
- *Detached spikes*: Spontaneous high voltage discharges that appear in no discernable pattern (neither tonic nor bursting).
- *Slow bursts*: Signals show bursting spike activity of up to more than a second. Bursts are separated by pauses that can have the same length of a second or more. Intra-burst spike rate is mostly low.
- *Detached bursts*: Bursting signal behavior with bursts of less than 500 ms with mostly high frequency intra-burst spike rates and low background noise. Pauses between bursts can be a second or longer.
- *Bursting*: No detached bursts but rather continuous bursty discharge with short pauses of less than 250 ms and a tendency towards higher background noise.
- *High frequency discharge with bursts*: Signals are characterized by very high background activity and continuous but irregular spiking that can be slightly bursting.
- *Low frequency tonic*: Regular discharge with relatively large interspike intervals.
- *High frequency tonic*: Regular discharge with smaller interspike intervals.

In many cases, mixtures between the above MER types were observed in the form of rapid changes in signal appearance or overlapping patterns. In these instances, an unambiguous classification might not be possible.

Although it would be desirable to reliably detect each of the listed MER types using an automatic classifier in order to further characterize MER trajectories encountered in DBS for dystonia or to develop a navigation assistant, as a first step, only a distinction between neuronal and non-neuronal MERs was attempted. We considered a recording to be neuronal if it belonged to any of the classes except *non-neuronal*. Because of the great variability among these classes, features were required that adequately cover all possible cases.

2.3 Feature Extraction

A number of features were considered for the classifier, some of which have been described in the literature and some of which are novel features. Because of the great variability of value ranges, mean-variance-normalization is applied to the extracted features. Furthermore, a modified natural logarithm is applied in case of the wavelet activity, which exhibits a positively skewed distribution of values. The features that were extracted are introduced in the following sections.

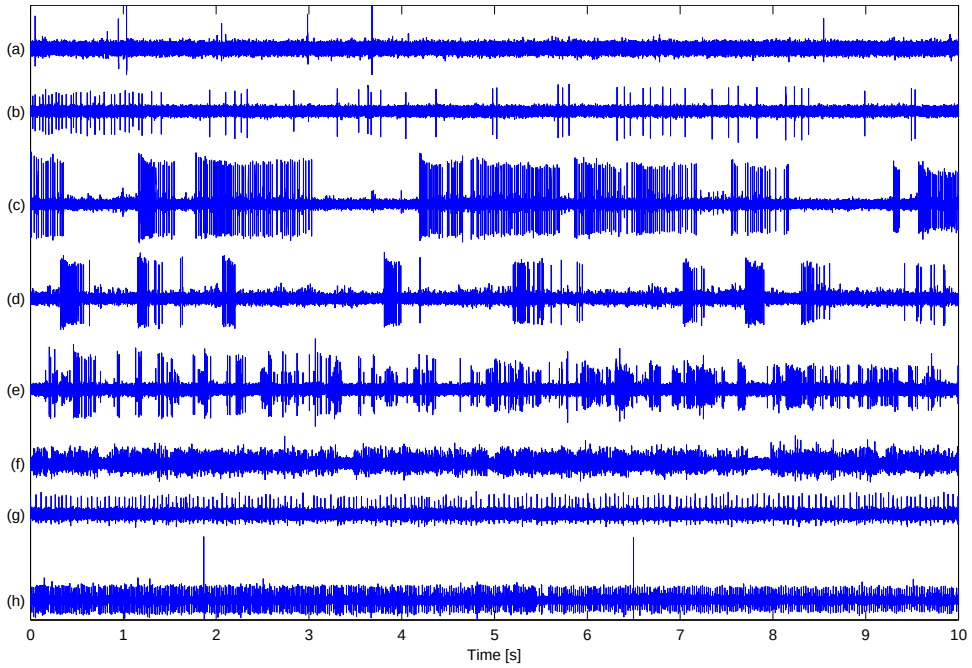

Figure 1. MER types: (a) Non-neuronal, (b) detached spikes, (c) slow bursts, (d) detached bursts, (e) bursting, (f) high frequency discharge with bursts, (g) tonic, low frequency, (h) tonic, high frequency.

2.3.1 Spike-dependent Features

Spike detection is done by thresholding the normalized cumulative energy difference (NCED), a method that is based on the slope of the cumulative sum of the squared input signal [15]. It requires no patient- or signal-specific thresholds and detects spikes of varying amplitudes with minimum configuration. For a MER s of length N, the normalized cumulative energy (NCE) $E(t)$ and its derivative (NCED) $E'(t)$ can be calculated as follows:

$$E(t) = \frac{\sum_{i=0}^{t} s(i)^2}{\sum_{i=0}^{N} s(i)^2}$$

$$E'(t) = \frac{E(t+1) - E(t-1)}{2}$$

The normalized cumulative energy difference is then thresholded using a fixed value τ_S. A high value of $E'(t)$ indicates a spike in the input MER.

$$M_{Spikes} = \{t | E'(t) > \tau_S\}$$

The waveform of a single action potential usually stretches across several neighbouring samples. Because this will most likely cause multiple spikes to be detected, adjacent spikes which fall into a certain window are merged, keeping the spike with the highest absolute amplitude.

We considered the following measures based on the detected spikes and interspike intervals (ISI):

1. *Spike rate (SR)*: Number of spikes per second.

2. *Burst Index (BI)*: Ratio of the number of interspike intervals shorter than τ_B to the number of interspike intervals longer than τ_B.

3. *Pause Index (PI)*: Ratio of the number of interspike intervals longer than τ_P to the number of interspike intervals shorter than τ_P.

4. *Pause Ratio (PR)*: Ratio of the time spent in pauses (interspike intervals longer than τ_P) to the time outside of pauses (interspike intervals shorter than τ_P).

5. *Tonicity (TS)*: The tonicity score attempts to measure signal regularity. It is based on the idea, that in a signal with regular spiking, the corresponding interspike intervals will be similar to each other. The tonicity score is defined as the relationship between ISI standard deviation and ISI mean:

   $$TS = \frac{\sigma_{ISI}}{\overline{ISI}}$$

   A low tonicity score indicates a tonic signal while a high value indicates irregular firing [10].

6. *Sub Spike Rate (subSR) / Sub Activity (subAct)*: The sub spike rate is defined as the mean number of spikes in the most active parts of a signal (those intervals that contain the most spikes). Its main intention is to measure sporadic neuronal activity appearing only in some disjoint regions of the complete signal, although it will

also exhibit high values for continuously firing neurons.

For the feature calculation the MER is split into equally sized sub signals that may be overlapping. For each of the sub signals, the number of spikes it contains is determined. The sub activity is defined as the mean of the highest spike rates of intervals that are a certain number of samples apart. By making sure that the sub signals used in the calculation are not too close to each other, it is guaranteed that the sub signals don't all belong to the same (short) burst, as one burst might not be enough of an indicator that the complete signal should be classified as neuronal.

The sub activity feature is similar to the sub spike rate in that it calculates the mean spike rates of a number of sub signals of the complete MER. However, the variance of signal intervals is used to find the most active sub signals.

7. *Burst Ratio*: The burst ratio (BR) is defined as the time spent in bursts divided by the signal length. Bursts are detected using a modified NCED method based on the interspike intervals. A burst in the input signal is represented by a flat slope in the derivative of the normalized cumulative sum of the interspike intervals. If several values in this derivative fall below a threshold, the spikes corresponding to the involved ISIs are noted to be forming a burst.

2.3.2 Spike-independent Features

1. *Activity*: The activity (ACT) feature measures the MER's background activity, based on percentiles and standard deviation. By using thresholds that are calculated from the data collected in the current recording session and not just from each individual signal, the activity feature is patient-specific and the recordings are analyzed in the context of the complete trajectory or multiple trajectories [8]. The feature extraction basically consists of two steps.

   (a) Threshold calculation: Two thresholds are calculated, t_q being a threshold derived from the signal percentiles P_x, and t_σ a threshold derived from the standard deviations. All the recordings $s_i \dots s_M$ being analyzed are included in the threshold calculation.

   $$t_q = P_\alpha(P_\beta(abs(s_1)), \dots, P_\beta(abs(s_M)))$$
   $$t_\sigma = P_\gamma(\sigma_1, \sigma_2, \dots, \sigma_M)$$

   with $0 \leq \alpha, \beta, \gamma \leq 100$.

   (b) Feature calculation: Each recording is divided into I_1 subsignals. $s_{i,k}$ being the k-th interval in the i-th signal and $\sigma_{i,k}$ being the standard deviation of $s_{i,k}$, the actual feature value ACT_i for each signal s_i is calculated as follows:

   $$ACT_i = \sum_{k=1}^{I_1} \left(\left(P_\beta \left(abs(s_{i,k}) \right) - t_q \right) + \left(\sigma_{i,k} - t_\sigma \right) \right)$$

2. *Wavelet Activity*: The wavelet activity (WVA) is based on the signal's variance. In order to analyze the signals with the least noise possible, the recordings are denoised using wavelet transformations (denoising by soft-thresholding) and subsequently decomposed. The produced wavelet-coefficients are split into I_2 intervals. The wavelet activity is defined as a percentile P_δ of variances of the wavelet coefficients w_i in these intervals:

   $$WVA = P_\delta \left(Var(abs(w_1)), \dots, Var(abs(w_{I_2})) \right)$$

   with $0 \leq \delta \leq 100$ [8].

3. *Cumulative Sum Coefficient*: The cumulative sum coefficient (CSC) attempts to measure the ratio of neuronal discharge and background noise. First the signal is sorted backwards. For the rest of the calculation, only the first F samples are kept and the normalized cumulative sum x_i^* of the cropped signal $\widehat{x}$ is computed:

   $$x_i^* = \frac{\sum_{j=1}^{i} \widehat{x}_j}{\sum \widehat{x}}$$

   Sorting backwards and cropping the signal causes negative samples to be disregarded. The cumulative sum coefficient is defined as the position of the sample where the normalized cumulative sum x^* first exceeds a threshold $\tau_{CSC} \in [0, 1]$. The resulting value is then divided by F, yielding a feature value between 0 and 1.

   $$CSC = \frac{\min\left(\{i | x_i^* > \tau_{CSC}\}\right)}{F}$$

   A low CSC value indicates a high spike-to-background amplitude ratio and suggests that the signal in question may be neuronal, a value close to one on the other hand indicates either low activity or very high firing rate and background noise.

4. *Amplitude ratio (amplRatio)*: Ratio of spike amplitudes and amplitudes of non-spike samples.

5. *Additional features*: Zero-Crossings, Curve Length, Peaks, Average Nonlinear Energy (NLE) [16].

2.4 Feature Selection

An initial look at the distribution of feature values gives some hints as to which features may have some relevance and which will most likely be of no use whatsoever. Figure 2 shows means and standard deviation for a subset of the calculated features. Some features, such as the number of zero crossings (*zCross*), the burst index (*BI*) and the number of peaks (*peaks*), are obviously unfit for class separation. Spike rate (*SR*), pause index (*PI*) and pause ratio (*PR*) on the other hand appear to be quite well-suited for differentiating between neuronal and non-neuronal. While

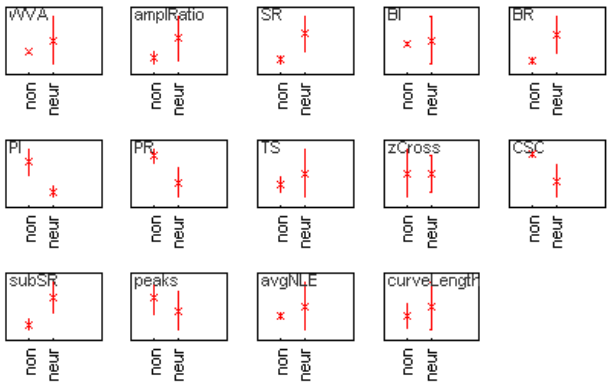

Figure 2. Feature distributions.

they are definitely valid indicators in the case of very typical signals, they fail to produce conclusive values, if the analyzed signals are not ideal examples of neuronal and non-neuronal recordings.

In the following we consider geometric mapping of features in the space of class representatives instead of classical (e.g. statistical) methods for feature selection.

2.4.1 Self-Organizing Maps (SOM)

Self-Organizing Maps (SOMs) are artificial neuronal networks based on unsupervised learning. A SOM consists of neurons representing weight vectors (prototype vectors, codebook vectors) organized on a regular low-dimensional grid. A SOM can be thought of as a net which is adjusted to the properties of the data cloud (the training data). In the trained map, neighboring neurons receive similar weight vectors that may form clusters which correspond to clusters in the input data. The training procedure roughly works as follows: The d-dimensional weight vectors $v_i = \left(v_i^1 v_i^2 \dots v_i^d\right)^t$ of the map's neurons are initialized with random values. During the training process, input vectors $x_j = \left(x_j^1 x_j^2 \dots x_j^d\right)^t$ are randomly drawn from the training data set and the neuron whose weight vector is closest to the input vector, the best-matching unit (BMU), is determined:

$$\|x_j - v_{BMU}\| = \min_i(\|x_j - v_i\|)$$

Once the best-matching unit has been identified, the underlying weight vector v_{BMU} as well as the weight vectors of the neighboring neurons are drawn closer to the input vector x_j, according to a given learning rate and neighborhood kernel. Iteratively presenting training vectors to the SOM, causes the map to gradually adjust to the training data [17].

After training the SOM with selected input features, the map is visualized with different information superimposed. (1) The *U-matrix* (figure 3, top left) visualizes distances between neighboring map units. High values in the U-matrix indicate a cluster border whereas low values are

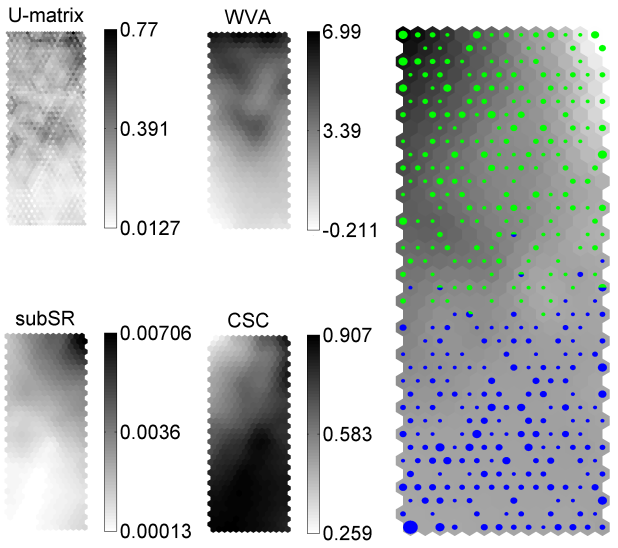

Figure 3. SOM trained with three selected features. Left: U-matrix and component planes, right: Hit/color plane with neuronal cluster (top) and non-neuronal cluster (bottom).

characteristic for the clusters themselves. (2) *Hit planes* (figure 3, right) show the distribution of best-matching units (the neuron whose weight vector is closest to an input vector) when presenting training or testing data to the trained map. The hits are shown as pie charts drawn on top of the neurons with the manual classification shown as pie colors and the size of the pie chart indicating how many data samples hit a certain neuron. (3) *Component planes* (figure 3, center) color code the values of each neuron's weight vector for a single feature. When looking at clusters on hit planes, component planes show which feature values are characteristic for a certain cluster and which features are redundant or irrelevant. (4) *Color planes* (figure 3, right) show the SOM in colors that represent the similarity between neighboring neurons according to a certain distance measure. Uniformly colored areas indicate that the underlying prototype vectors are similar. In combination with a hit plane, one can see whether the formed hit clusters are well-separated.

After subsequently narrowing down the features used to train the SOM, wavelet activity, sub spike rate and cumulative sum coefficient emerged as the most effective measures for distinguishing non-neuronal and neuronal recordings. As the color plane on the right of figure 3 shows, a neuronal cluster has formed at the top and a non-neuronal cluster at the bottom. The U-matrix shown in the top left indicates a fairly large diversity of weight vectors in the neuronal cluster and a more uniform distribution in the non-neuronal cluster. Together with the component planes, the two signal groups can be further characterized. Non-neuronal MERs generally have low values for wavelet activity and sub spike rate and a high cumulative sum coeffi-

cient. The neuronal cluster can be split into two sub clusters. They both share a medium or high wavelet activity and either a very low cumulative sum coefficient (top left part of map) or a high cumulative sum coefficient but a high sub spike rate (top right part of map).

2.5 Fuzzy Classifier

Using the three features that proved to be especially well-suited for differentiating neuronal and non-neuronal recordings in the SOM analysis, we constructed a Takagi-Sugeno type fuzzy classifier. While an automatic creation of a fuzzy system and the used membership functions using subtractive clustering and subsequent linear least squares optimization (as provided by Matlab™function `genfis2`) for these three features yielded fair results, the resulting systems tended to deliver unstable output when presented with testing data that differed much from the training data or when classifying recordings with uncommon feature combinations (i.e. outliers). This may be a consequence of the constraints of automatic fuzzy system generation, such as (1) the usage of Gaussian input membership functions that are unable to adequately cover extreme feature values, (2) linear combination of inputs that may cause undesirable output if unexpected feature values (e.g. extremes) are presented to the system, (3) generation of one rule for every cluster found in the training data, which renders the resulting system inflexible, (4) usage of all features in all rules although certain clusters are characterized more easily using only a subset of the features and (5) the inability of incorporating expert knowledge obtained from previous research.

The fuzzy classifier was therefore adapted to use asymmetrical Gaussian curves as input membership functions where extremes need to be incorporated and constant output functions that are insensitive to unexpected input feature combinations. The rules used in the classifier are shown in table 1. The first three columns contain the input feature ranges that cause a rule to fire (rule antecedents, and-connected) while the fourth column shows the corresponding consequents, *neur* being constant 1 and *non* being constant 0. A high wavelet activity value will for example cause the second rule to fire, shifting the overall output of the system towards *neur*. The linguistic terms used on the antecedent side correspond to input membership functions that are laid out according to information gained from performing subtractive clustering on the training data.

The adapted system is then trained using a combination of the least-squares method and the backpropagation gradient descent method (Matlab™function `anfis`) in order to fine-tune the system's membership function parameters.

2.6 Results

Of initially 16 features, the most promising three were selected and a fuzzy classifier was automatically generated.

WVA	subSR	CSC	Output
		low	neur
high			neur
medium to high	high	medium to high	neur
low	low	high	non

Table 1. Adapted fuzzy rules. $neur = 1$, $non = 0$.

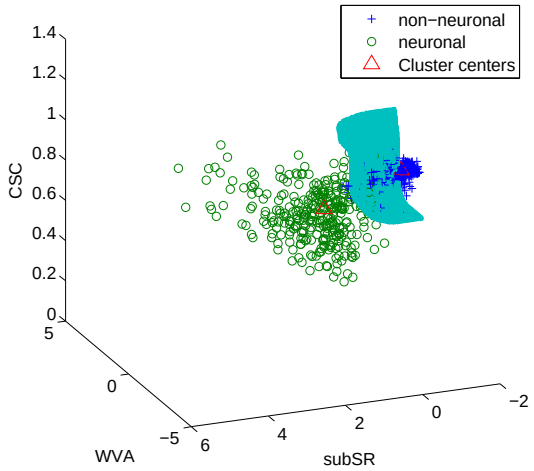

Figure 4. Approximate discriminant function of the classifier.

The system was then presented with testing data (n=691, n_{non}=365, n_{neur}=326), which it successfully divided into the expected classes as can be seen in figure 4.

3 Conclusion

In this study, we examined microelectrode recordings from pallidal DBS in dystonia which proved to be very diverse as has already been reported by others. We grouped the recordings into types and extracted several features which were then narrowed down to those that best differentiate neuronal from non-neuronal recordings. Using information obtained from SOM analysis, a fuzzy classifier was constructed that allows for a good automatic distinction between the two classes. The performance of the classifier indicates that the chosen features are well suited for the classification task. However, the classifier fails in some cases, mostly when presented with outliers exhibiting uncommon feature combinations. Although these cases can possibly be detected using additional features, we intend to keep the system dimension as low as possible, favoring a deterministic system.

In future investigations, several aspects could be of interest. A simplification of the used set of rules, e.g. by combining the three rules for *neuronal* could further improve classifier performance. For pathological cases in which the classifier fails, it needs to be determined why that is and how the system can be adapted to deal with these cases ad-

equately. It might be the extracted features that fail, which would suggest the need for improvement of some of the used measures, or there may be other reasons for the misclassification, such as artefacts (visible and invisible) or clipping of the analyzed microelectrode recordings. Furthermore, the sudden variations of signal types encountered along many of the trajectories used in this study suggest that the chosen distance of $0.5 - 1.0$ mm between recordings needs to be decreased so structure borders are easier to detect, as this can be an essential indicator for identifying the stimulation target.

References

[1] P.A. Starr, R.S. Turner, G. Rau, N. Lindsey, S. Heath, M. Volz, J.L. Ostrem, & W.J. Marks, Microelectrode-guided implantation of deep brain stimulators into the globus pallidus internus for dystonia: Techniques, electrode locations, and outcomes, *Journal of Neurosurgery*, *104*(4), 2006, 488-501.

[2] W.D. Hutchinson, Techniques of microelectrode recording in movement disorder surgery, in J.K. Krauss, J. Jankovic, & R.G. Grossman (Ed.), *Surgery for Parkinson's Disease and Movement Disorders*, (Philadelphia: Lippincott Williams & Wilkins, 2001) 110-118.

[3] M.L. Bootin, Deep brain stimulation: Overview and update, *Journal of Clinical Monitoring and Computing*, *20*(5), 2006, 341-346.

[4] A. Priori, M. Egidi, A. Pesenti, M. Rohr, P. Rampini, M. Locatelli, F. Tamma, E. Caputo, V. Chiesa, & S. Barbieri, Do intraoperative microrecordings improve stn targeting in stereotactic neurosurgery for parkinsons disease?, *Journal of Neurosurgery*, *47*(1), 2003, 56-60.

[5] P.A. Starr, Placement of deep brain stimulators into the subthalamic nucleus or globus pallidus internus: Technical approach, *Stereotactical and Functional Neurosurgery*, *79*(1), 2002, 118-145.

[6] T. Yokoyama, K. Sugiyama, S. Nishizawa, T. Tanaka, N. Yokota, S. Ohta, & K. Uemura, Neural activity of the subthalamic nucleus in parkinson's disease patients, *Acta Neurochir*, *140*(12), 1998, 1287-1291.

[7] P. Zhuang & Y.-J. Li, Characteristics of subthalamic neuronal activities in parkinson's disease, *Acta Physiologica Sinica*, *55*(4), 2003, 435-441.

[8] P. Gemmar, M.E. Tercero, T. Henrichs, Y. Thesen, O. Gronz, & F. Hertel, Fuzzy classifier for microelectrode recording-based target navigation in deep brain stimulation, *Proceedings of Curac 2008*, Leipzig, Germany, 2008.

[9] J.K.H. Tang, E. Moro, N. Mahant, W.D. Hutchison, A.E. Lang, A.M. Lozano, & J.O. Dostrovsky, Neuronal firing rates and patterns in the globus pallidus internus of patients with cervical dystonia differ from those with parkinsons disease, *Journal of Neurophysiology*, *98*(1), 2007, 720-729.

[10] M. Merello, D. Cerquetti, A. Cammarota, E. Tenca, C. Artes, J. Antico, & R. Leiguarda, Neuronal globus pallidus activity in patients with generalised dystonia, *Movement Disorders*, *19*(5), 2003, 548-554.

[11] M.K. Sanghera, R.G. Grossman, C.G. Kalhorn, W.J. Hamilton, W.G. Ondo, & J. Jankovic, Basal ganglia neuronal discharge in primary and secondary dystonia in patients undergoing pallidotomy, *Neurosurgery*, *52*(6), 2003, 1358-1373.

[12] C.M. Magarinos-Ascone, I. Regidor, M. Gómez-Galán, L. Cabanes-Martínez, & R. Figueiras-Méndez, Deep brain stimulation in the globus pallidus to treat dystonia: Electrophysical characteristics and 2 years' follow-up in 10 patients, *Neuroscience*, *152*(2), 2008, 558-571.

[13] P. Zhuang, Y. Li, & M. Hallett, Neuronal activity in the basal ganglia and thalamus in patients with dystonia, *Clinical Neurophysiology*, *115*(11), 2004, 2542-2557.

[14] M. O. Pinsker, J. Volkmann, D. Falk, J. Herzog, F. Steigerwald, G. Deuschl, & H. M. Mehdorn, Deep brain stimulation of the internal globus pallidus in dystonia: target localisation under general anaesthesia, *Acta Neurochir*, *151*(7), 2009, 751-758.

[15] N. Mtetwa & L.S. Smith, Smoothing and thresholding in neuronal spike detection, *Neurocomputing*, *69*(10-12), 2006, 1366-1370.

[16] J.L. Jaggi, S. Wong, G.H. Baltuch, & S.F. Danish, Functional localization and visualization of the subthalamic nucleus from microelectrode recordings acquired during dbs surgery with unsupervised machine learning, *Journal of neural engineering*, *6*(2), 2009, 26006-26016.

[17] J. Vesanto, J. Himberg, E. Alhoniemi, & J. Parhankangas, Self-organizing map in matlab: the som toolbox, *Proceedings of the Matlab DSP Conference 1999*, Espoo, Finland, 1999, 35-40.